

Using Wavelet Analysis to Detect Tornadoes from Doppler Radar Radial-Velocity Observations

SHUN LIU

Center for Analysis and Prediction of Storms, University of Oklahoma, Norman, Oklahoma, and College of Atmospheric Sciences, Lanzhou University, Lanzhou, China

MING XUE

Center for Analysis and Prediction of Storms and School of Meteorology, University of Oklahoma, Norman, Oklahoma

QIN XU

NOAA/National Severe Storms Laboratory, Norman, Oklahoma

(Manuscript received 25 October 2005, in final form 11 July 2006)

ABSTRACT

A wavelet-based algorithm is developed to detect tornadoes from Doppler weather radar radial-velocity observations. Within this algorithm, a relative region-to-region velocity difference (RRVD) is defined based on the scale- and location-dependent wavelet coefficients and this difference represents the relative magnitude of the radial velocity shear between two adjacent regions of different scales. The RRVD fields of an idealized tornado and a realistic tornado from a high-resolution numerical simulation are analyzed first. It is found that the value of RRVD in the tornado region is significantly larger than those at other locations and large values of RRVD exist at more than one scale. This characteristic forms the basis of the new algorithm presented in this work for identifying tornadoes. Different from traditional tornadic vortex signature detection algorithms that typically rely on the velocity difference between adjacent velocity gate pairs at a single spatial scale, the new algorithm examines region-to-region radial wind shears at a number of different spatial scales. Multiscale regional wind shear examination not only can be used to discard a nontornadic vortex signature to reduce the false alert rate of tornado detection but also has the ability of capturing tornadic signatures at various scales for improving the detection and warning. The potential advantage of the current algorithm is demonstrated by applying it to the radar data collected by Oklahoma City, Oklahoma (KTLX), Weather Surveillance Radar-1988 Doppler (WSR-88D) on 8 May 2003 for a central Oklahoma tornado case.

1. Introduction

Modern Doppler radars have the ability to scan large volumes of the atmosphere at high space and time resolutions. Such measurements have provided unprecedented opportunities for detecting small-scale hazardous weather phenomena such as tornadoes. A number of algorithms (e.g., Mitchell et al. 1998; Desrochers and Donaldson 1992; Wieler 1986; Vasiloff 2001) have been developed over the years to automatically identify tornado from radar reflectivity and/or radial velocity by

examining hook echoes (Fujita 1958; Browning 1965) and tornadic vortex signatures (TVSs; Burgess et al. 1975; Crum and Alberty 1993). Among them, the tornado detection algorithms based on hook echoes alone are usually not reliable enough (e.g., Forbes 1981; Mitchell et al. 1998). Newer algorithms, such as the National Severe Storms Laboratory Tornado Detection Algorithm (NSSL TDA, referred to as NTDA hereafter; Mitchell et al. 1998) and the past operational Weather Surveillance Radar-1988 Doppler (WSR-88D) TVS algorithm, are based primarily on TVSs identified from the radial velocity data.

TVS is primarily quantified by gate-to-gate azimuthal shear (Burgess et al. 1975; Brown et al. 1978). With the WSR-88D TVS algorithm, the presence of a mesocyclone is required. The algorithm is invoked after a me-

Corresponding author address: Shun Liu, Environmental Modeling Center, National Centers for Environmental Prediction, Room 207, 5200 Auth Rd., Camp Springs, MD 20746.
E-mail: Shun.Liu@noaa.gov

socyclone is detected by the mesocyclone detection algorithm (MDA), and it searches in and around the mesocyclone at each elevation angle for inbound and outbound velocity extrema. When the shear between the velocity extrema exceeds a certain threshold (default is 0.02 s^{-1}) at two or more elevation angles, a TVS is declared and it is automatically assumed to be tornadic (see, e.g., Mitchell et al. 1998). With the newer NTDA, the presence of a mesocyclone is not required, and therefore the detection of nonsupercell tornadoes is not excluded. The algorithm identifies vortices via examination of the gate-to-gate azimuthal (adjacent in azimuth and constant in range) velocity differences (GVDs; Mitchell et al. 1998), using low thresholds first; it then attempts to classify them as either tornadic or nontornadic. Three-dimensional (3D) regions with GVD exceeding certain thresholds are constructed and certain characteristics of such 3D regions are then used to determine the tornadic nature of the 3D detection. The NTDA was found to have a much higher probability of detection (POD) than the WSR-88D TVS algorithm while still keeping the false alarm rate (FAR) reasonable.

These existing TVS detection algorithms rely heavily on the velocity differences between two adjacent gate pairs; there exist, however, many uncertainties with the estimation and use of such velocity differences, due to radar data noise, the azimuthal offset of sample volumes from the center of the rotation features (Wood and Brown 1997), natural small-scale variations in the flow (Desrochers and Yee 1999), and other data quality problems (Zittel et al. 2001). These problems can create spuriously large velocity differences or strong azimuthal shears that can significantly increase the false alarm rate. In addition, because tornado size and intensity vary, it is difficult to set thresholds based primarily on GVDs that work for all cases (Desrochers and Yee 1999). The discrete sampling of the atmosphere by radar whose sampling resolution changes with the range and whose beam positioning relative to the vortex center affects GVD values further complicates the issue. It would be very helpful if additional discriminating parameters could be found that would better define the characteristics of tornadoes and their associated vortices. Ideally, such parameters are insensitive to the aforementioned problems. Finding such parameters is the motive of this study.

Since the azimuthal shear signatures associated with tornadoes as seen in Doppler radial velocity data are often not confined to two adjacent radar gates in the azimuth, the shear or velocity difference between larger distances (compared to the adjacent radar gate distance in the azimuth) or between regions can provide valu-

able information that can potentially be utilized to reduce the false alarm rate of detection. In this paper, we use the wavelet analysis technique for the quantification of velocity differences at different spatial scales and use these measures to help design or improve tornado detection algorithms. In particular, a set of wavelet basis functions will be used and each basis function describes the averaged radial-velocity difference between two adjacent regions covered by this basis function. By applying the wavelet analysis to the radial velocity field, a region-to-region velocity difference (RVD) can be defined in terms of the wavelet coefficients. When normalized, the relative region-to-region velocity difference (RRVD) for each scale can be obtained. If the relative difference is larger than a certain threshold value, then the region at the corresponding scale can be considered as having a significant radial wind shear and a high potential for containing a tornado. The normalization allows for a more general determination of the threshold without depending too much on or being too sensitive to the tornado intensity information.

For similar reasons noted above, Smith et al. (2003) and Smith and Elmore (2004) recently showed that a local, linear, least square approach to calculating the radial velocity derivatives, including the azimuthal shear, leads to a significant improvement over the typically used method of calculating the shear from two data points. With the approach, a least square estimation of the shear in a local region that includes a number of radial velocity data points is performed to improve the reliability of the shear estimate. There is a certain similarity between our wavelet-analysis approach and their approach, in that both methods utilize radial velocity data at more than two neighboring data points. Our approach further examines the shear magnitudes at more than one scale.

This paper is organized as follows. In section 2, wavelet analysis is introduced and scale-dependent RRVD is defined. Analyses are performed on radial velocity data sampled from an idealized tornado and from a realistic tornado from a high-resolution numerical simulation. A tornado detection algorithm based on RRVD and other parameters is proposed in section 3 and applied to a real tornado case in section 4. Conclusions are given in section 5.

2. Wavelet analysis and applications to radial-velocity fields

a. Wavelet transform

Similar to the commonly used Fourier transform, the wavelet transform is a method of converting a function

(or signal) into another form or representation, usually in terms of the wavelet coefficients, that would allow certain features of the original signal more amenable to study or enable the original dataset to be described more succinctly (Daubechies 1992). In the case of a Fourier transform, the coefficients of different Fourier components reveal the strength or intensity of the signal at different wavelengths or frequencies. The meaning of the wavelet coefficients depends very much on the choice of the wavelet basis function used, which has wide variations.

The wavelet transform of a spatial function (or signal) $f(\mathbf{x})$ in two dimensions can be defined in general by

$$W(s, \mathbf{l}) = \int f(\mathbf{x})\psi_{s,\mathbf{l}}(\mathbf{x}) d\mathbf{x}, \quad (1)$$

where \mathbf{x} and \mathbf{l} are vectors, $\mathbf{x} = (x, y)$ and $\mathbf{l} = (l_x, l_y)$, and x and y , l_x and l_y (all are real) are independent spatial variables. Here, $\mathbf{x} = (x, y)$ defines the spatial coordinates of the original function whereas $\mathbf{l} = (l_x, l_y)$ defines the location at which the local wavelet basis function, $\psi_{s,\mathbf{l}}(\mathbf{x})$, is centered. We use $W(s, \mathbf{l})$ to represent the wavelet transform coefficients at scale s and location \mathbf{l} .

The wavelet functions, denoted by $\psi_{s,\mathbf{l}}(\mathbf{x})$, are constructed by shifting and dilating a wavelet prototype function $\psi(\mathbf{x})$, and $\psi_{s,\mathbf{l}}(\mathbf{x})$ can be expressed as

$$\psi_{s,\mathbf{l}}(\mathbf{x}) = p(s)\psi\left(\frac{\mathbf{x} - \mathbf{l}}{s}\right). \quad (2)$$

The wavelet coefficient W represents the correlation between the original signal and the corresponding wavelet basis function or the amount of energy in the signal at scale s and location \mathbf{l} . Here, $p(s)$ is a weighting function, which is typically $p(s)$ set to $1/\sqrt{s}$ for energy conservation.

For discrete signal analyses, we need to use discrete wavelet transform algorithms (e.g., Daubechies 1992). The discretization of the wavelet basis function has the form of

$$\psi_{m,\mathbf{n}}(\mathbf{x}) = \psi\left(\frac{\mathbf{x} - \mathbf{n}}{s_0^m}\right), \quad (3)$$

where integers m and $\mathbf{n} = (n_x, n_y)$ are used instead of the continuous s and \mathbf{l} in Eq. (2) and they control the wavelet dilation and translation, respectively; s_0 is a specified fixed dilation step parameter (≥ 1). The wavelet transform is then

$$W_{m,\mathbf{n}} = p(m) \int f(\mathbf{x})\psi_{m,\mathbf{n}}(\mathbf{x}) d\mathbf{x}, \quad (4)$$

and $W_{m,\mathbf{n}}$ is the discrete version of the wavelet transform coefficient corresponding to scales and locations represented by m and \mathbf{n} .

According to the above formulations, the wavelet basis function can be moved to or defined at different locations of the data field. In our case, for analyzing radar observations, the basis function can be shifted in the azimuthal and radial directions. The basis function itself also can be stretched or compressed, as described by Eqs. (2) and (3). By using (1) or its discrete version in (4), the wavelet transform quantifies the local match of the wavelet function with the original function or field $f(x)$. When the wavelet matches the shape of the function well at a specific scale and location, a large wavelet coefficient W is obtained. Just the opposite takes place when the wavelet and function do not correlate well, as a low value of coefficient W is obtained. Thus, using the wavelet transform, a map of local correlations between the wavelet (at various scales and locations) and the analyzed field can be obtained. By checking the wavelet coefficients in the wavelet space, the information of the spatial structures of the field can be presented in a more useful form.

b. Relative region-to-region velocity difference

Within the Doppler radar radial velocity observations, a tornado usually appears as a couplet of enhanced incoming and outgoing radial velocities. Because tornadoes usually do not exist in isolation, the shear information associated with a tornado is often contained in more than two adjacent radial velocity sampling volumes or pixels of observations (Vasiloff 2001; Wood and Brown 1997). Here, a pixel corresponds to a radar sampling volume in the image form. Through wavelet analysis, it is possible to quantify azimuthal radial velocity differences between regions of different scales, and we can use the shear information at more than the gate-to-gate azimuthal shear scale alone to help improve tornado detection.

For the description of the azimuthal shear of radial velocity in an elevation plane in two dimensions, the 2D Harr wavelet is chosen in this study. Because the main purpose of our wavelet analysis is to highlight or extract the azimuthal shear information at multiple scales, the step-function-like Haar wavelet appears most suitable. This wavelet function is given by

$$\psi(\mathbf{x}) = \psi(x, y) = \begin{cases} 1 & 0 \leq x \leq \frac{1}{2}, 0 \leq y \leq 1 \\ -1 & \frac{1}{2} \leq x \leq 1, 0 \leq y \leq 1 \\ 0 & \text{elsewhere} \end{cases} \quad (5)$$

Note that in our case, x and y denote the azimuthal and radial directions, respectively. This wavelet basis function can be dilated to construct a set of wavelet functions representing different scales in the two dimensions. Such 2D wavelet functions can also be expressed as a series of matrices in discrete form using the dyadic-scale discretization. For example, the wavelet functions for the first two scales ($m = 1$ and 2) can be expressed in matrices as follows:

$$\psi_1 = \begin{bmatrix} 1 & -1 \\ 1 & -1 \end{bmatrix}, \quad \psi_2 = \begin{bmatrix} 1 & 1 & -1 & -1 \\ 1 & 1 & -1 & -1 \\ 1 & 1 & -1 & -1 \\ 1 & 1 & -1 & -1 \end{bmatrix}, \quad (6)$$

where the subscripts represent m . As can be seen, a 2D discrete Harr wavelet at scale $m = 2$ is a dilation in both the x and y directions from the wavelet at scale $m = 1$. The matrices in the above equations are mapped to the radial velocity data space, so that each element in the matrices corresponds to one radial velocity measurement while the centers of the matrices correspond to the central location where the wavelets are defined. The columns and rows correspond to the radial and azimuthal directions, respectively. The left half of the matrices is unity while the right half is negative unity. There is a jump between the left and right halves of the matrices, making them suitable for describing azimuthal shear features.

When a 2D wavelet function at a given scale is used, the wavelet coefficient can be used to measure the difference of the signal $f(\mathbf{x})$ across the two regions corresponding to the left and right halves of the discrete wavelet function. Applying such a wavelet transform to the Doppler radial velocity field, a large value of the wavelet coefficient at a given scale indicates the existence of a large velocity difference between the two adjacent regions. The sizes of the regions are $2^m \times 2^{m-1}$ pixels for scale m , and $p(m)$ in Eq. (4) is given by $p(m) = 1/(2^m \times 2^{m-1})$. We can obtain a wavelet coefficient for each scale m at each particular location that measures the region-to-region velocity difference (RRVD) at that location for the corresponding scale.

However, the intensity of the tornado vortex varies with cases and the wavelet coefficients vary with the scale so that it is still not easy to determine the general thresholds for separating a tornadic vortex from non-tornadic shear signatures. To make it easier to determine more general thresholds, we define here the normalized or relative wavelet coefficients for each scale according to

$$\text{RRVD}_{m,\mathbf{n}} = \frac{W_{m,\mathbf{n}}}{W_{m,\max}}, \quad (7)$$

where $W_{m,\max}$ is the maximum wavelet coefficient at scale m . $\text{RRVD}_{m,\mathbf{n}}$ measures the relative region-to-region velocity difference at scale m and location \mathbf{n} . The value of RRVD ranges from 0 to 1 at any scale. A large value of $\text{RRVD}_{m,\mathbf{n}}$ indicates the presence of a significant shear or a jump in the original signal between the two regions at scale m .

c. Wavelet analysis for an idealized vortex

To quantify the main RRVD characteristics of tornadoes and to determine the suitable RRVD thresholds for their detection, we first apply our wavelet analysis to an idealized tornado vortex, given by a modified Rankine combined vortex model as used by Brown et al. (2002):

$$V = V_x(R/R_x)^\lambda, \quad (8)$$

where V is the rotational velocity at radius R (from the vortex center) and V_x is the maximum rotational velocity at the core radius of R_x , and $\lambda = 1$ for $R \leq R_x$ and $\lambda = -0.6$ for $R > R_x$. For our sampling experiment in this section, we assume $R_x = 200$ m and $V_x = 50$ m s⁻¹, similar to Brown et al. (2002). The WSR-88D radial velocity simulation method of Wood and Brown (1997) is used here to simulate the radial velocity observations. Specifically, the radial velocity is sampled at 1° azimuthal intervals and at a 250-m range resolution. The center of the simulated vortex is located 20 km north of the radar. For simplicity, a 0° elevation angle (strictly speaking, the lowest elevation angle of the WSR-88D radar is 0.5°) and uniform reflectivity are assumed. For an effective sampling volume, the mean radial velocity $\bar{v}_r(\theta_0, r_0)$ at the range, r_0 , and the azimuth angle, θ_0 , are given, following Wood and Brown (1997), by

$$\bar{v}_r(\theta_0, r_0) = \frac{\sum_i^I \sum_j^J v_r(\theta_i, r_j) W(r)^2 f^4(\theta)}{\sum_i^I \sum_j^J W(r)^2 f^4(\theta)}, \quad (9)$$

where I and J are, respectively, the number of samples taken along the azimuth and range in the sampling volume, $v_r(\theta_i, r_j)$ is the radial velocity in the i th and j th sampling points, and $W(r)$ and $f(\theta)$ are the range and antenna pattern weighting function, respectively. Using (8), the u and v components of the wind in Cartesian coordinates are calculated first on a grid of 25-m resolution. The gridpoint values within a radar sample vol-

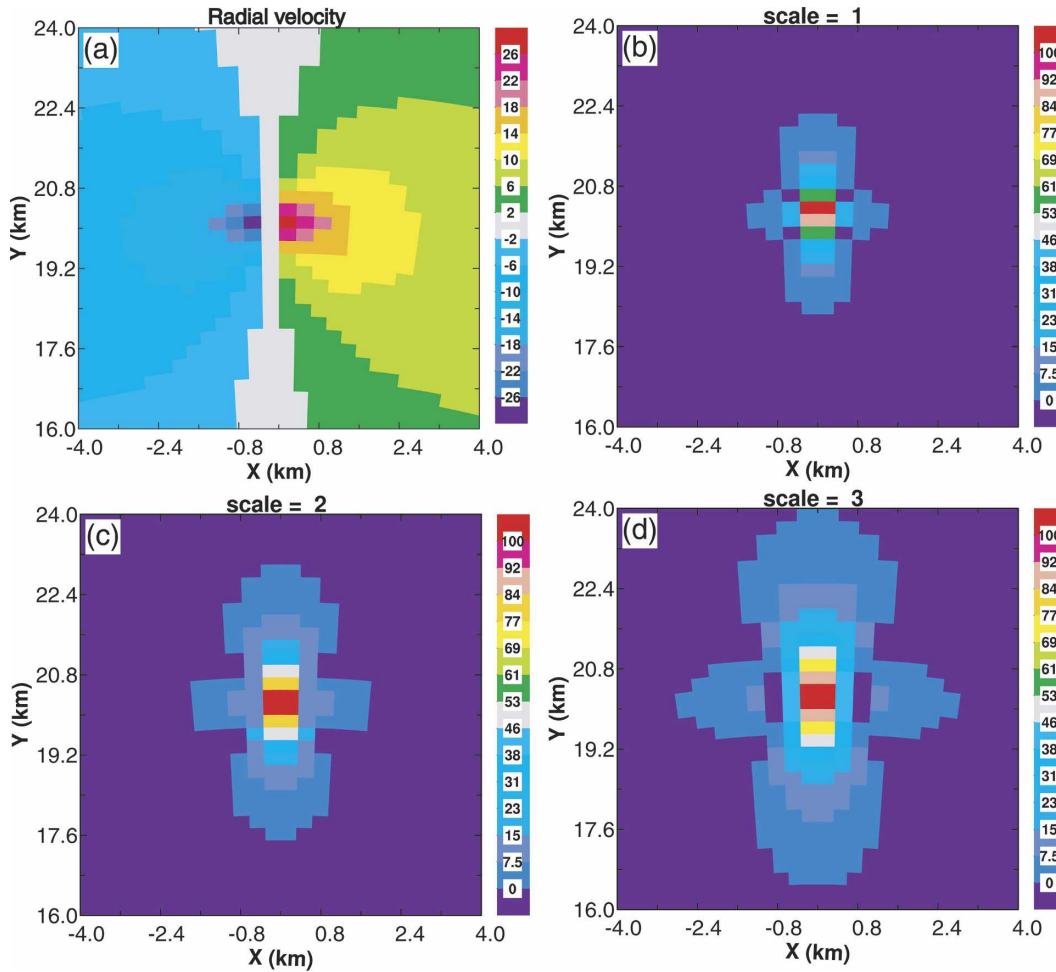


FIG. 1. (a) Simulated radial velocity field from the modified Rankine combined vortex and the corresponding RRVD (%) at scales $m =$ (b) 1, (c) 2, and (d) 3. The radar is 20 km south of the tornado, located at the coordinate origin.

ume are averaged, according to (9), to obtain the radial velocity observations, where $v_r(\theta_i, r_j)$ is given by

$$v_r(\theta_i, r_j) = u(\theta_i, r_j) \cos(\theta_i) + v(\theta_i, r_j) \sin(\theta_i). \quad (10)$$

For the simulation of radial velocity data, the angular effective beamwidth used is 1.39° , that of the WSR-88D, and the (linear) effective beamwidth (EBW) is 485 m at the 20-km range, which is larger than the core diameter of 400 m of this idealized vortex. TVS is therefore expected in the radial velocity field (Brown 1998). The simulated radial velocity field is shown in Fig. 1a. As can be seen, the radial velocity in the left half of the plotting domain is inbound relative to the radar and is therefore negative and that in the right half is positive. A large velocity difference exists across the central axis of the domain, through the vortex center, and the largest velocity difference occurs between two pixels separated by a pixel with nearly zero velocity. This is a TVS

that occurs when one of the beam centers coincide more or less with the vortex center (Brown 1998). The wavelet analysis described in section 2a is applied to this radial velocity field in the radar polar coordinates and the RRVDs are calculated from Eq. (7) for each scale and location. The RRVDs for $m = 1, 2,$ and 3 are plotted in Figs. 1b, 1c, and 1d, respectively. As can be seen, the RRVDs near the center of the vortex are larger than 50% for all three scales and are significantly higher than the values away from the vortex. In fact, the maximum values all exceed 90% near the center of the vortex, which should be the case by definition. The number of pixels whose RRVD is larger than 0.5 is 6 for scale $m = 1$ (Fig. 1b), 12 for scale $m = 2$ (Fig. 1c), and 16 for scale $m = 3$ (Fig. 1d). Therefore, the signature of the vortex increases in size in terms of RRVD as the scale of the RRVD increases. It is clear from this example that the multiscale characteristics of RRVD in

the tornado region are different from those in other regions, suggesting that the RRVDs at multiple scales can be useful for identifying a tornado vortex in radial velocity data. In practice, additional criteria will also be needed to unambiguously identify a tornado.

d. Wavelet analysis for a numerically simulated tornado

A much more realistic tornado simulated at high spatial resolution is available for further quantifying the characteristics of RRVD and determining their thresholds. This simulation was performed using the Advanced Regional Prediction System (ARPS; Xue et al. 2000, 2001), starting from a modified sounding for 20 May 1977 during a Del City, Oklahoma, tornadic supercell storm. A uniform horizontal resolution of 50 m was used together with a vertical stretched grid with a near-surface vertical resolution of 20 m. Over a half-hour centering on the period of most intense tornado activity, a uniform horizontal resolution of 25 m was used and the model domain was 48 km × 48 km in the horizontal. A maximum ground-relative wind speed of over 120 m s⁻¹, located about 30 m above the frictional ground, was obtained in the simulated tornado, with a pressure drop of over 80 hPa at the center of the tornado vortex. Detailed description and analyses of the simulations will be reported elsewhere. In this paper, we sample the ground-level flow of this simulated tornado in the same way as we did in the earlier idealized Rankine combined vortex case, again at an azimuthal resolution of 1° and at a range gate resolution of 250, with an elevation angle of 0.0°. The same 1.39° effective beamwidth is assumed. For the experiment reported in this section, the radar is located 20 km west of the domain center. The view from west is chosen because the elliptically shaded ground-level tornado vortex is narrower in the north–south direction (Fig. 2); the tornado is smaller when viewed from the east or west and is, therefore harder to detect. As can be seen, the core diameter of the simulated tornado in the north–south direction, as determined by the distance between the minimum and maximum east–west velocities associated with the tornado vortex, of about -20 and 35 m s⁻¹ (Fig. 2a), respectively, is about 200 m. This tornado, as

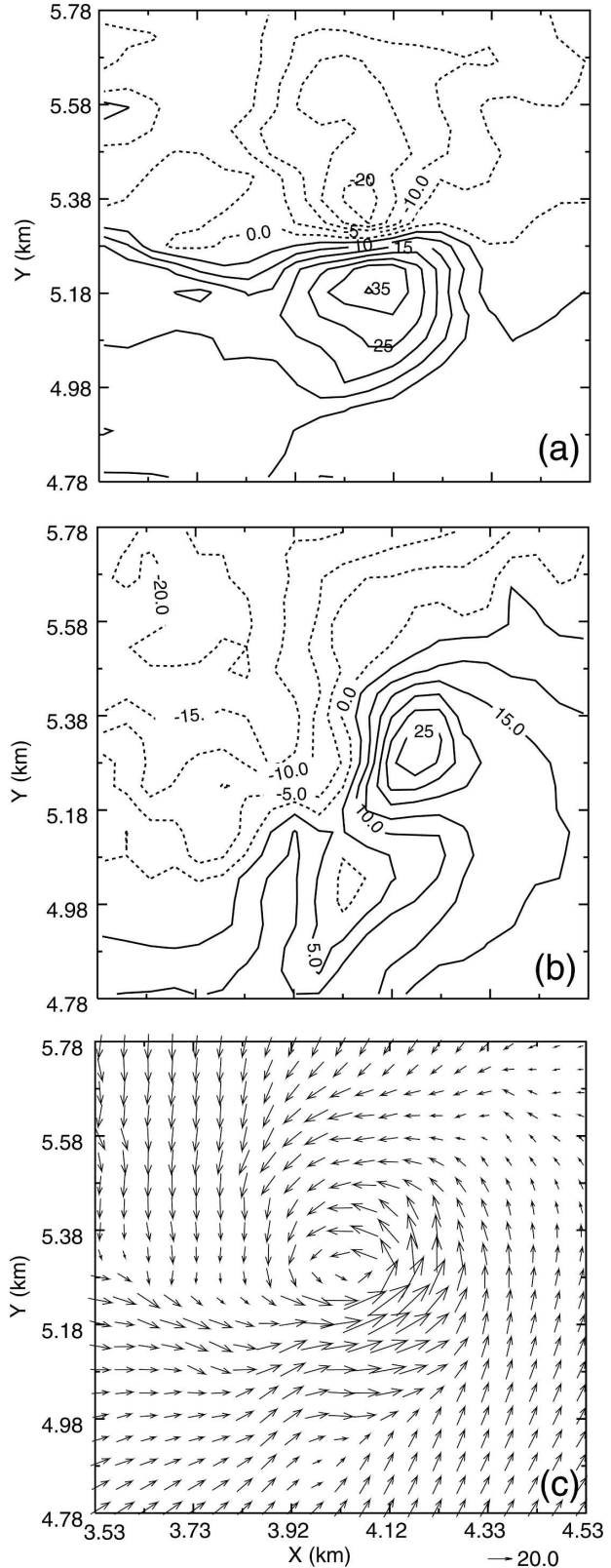


FIG. 2. The (a) east–west and (b) north–south velocity components of the ground-level winds and (c) wind vectors of a numerically simulated tornado that developed within a numerically simulated supercell storm. A 1-km-squared domain centered on the tornado is shown; the horizontal resolution of the numerical simulation was 25 m.

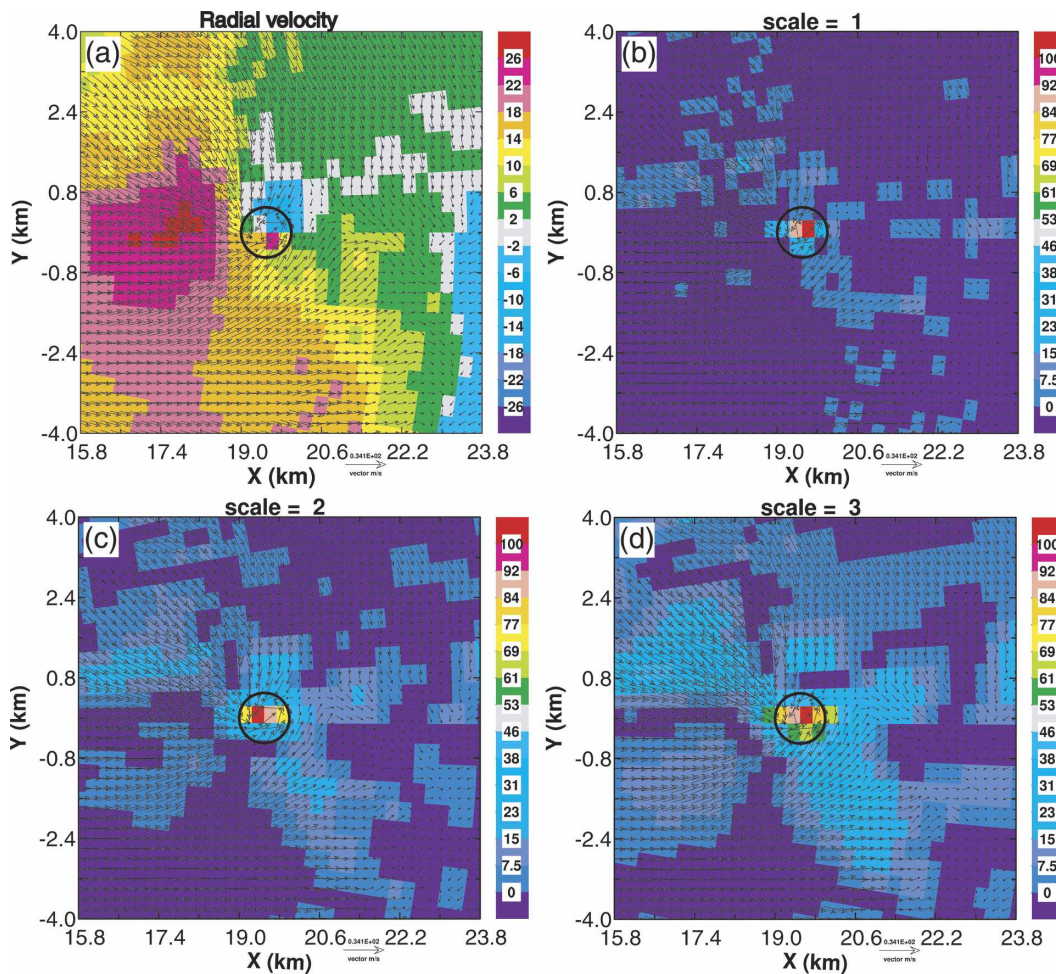


FIG. 3. As in Fig. 1, but for simulated radial velocities and the corresponding RRVDs from the numerically simulated tornado shown in Fig. 2. The radar is located 20 km west of the tornado.

seen at the ground level, is weaker than the idealized tornado of the previous section. The wind field in this case is also more complex than the case of the idealized vortex.

The simulated radial velocity field is shown in Fig. 3a, together with horizontal wind vectors. In this plot, the tornado is centered at (0, 20) km while the radar is located at the coordinate origin. There exists obviously strong convergence in the tornado region and a region of strong divergence northwest of the tornado that originated from the rear-flank downdraft. Apart from that, the general tornadic vortex features, as revealed by the radial velocity field, are similar to that of the idealized vortex case. The central part of the tornado is marked by a closed circle in the figure. Similar to the earlier idealized case, we can see a radial velocity couplet with a large velocity difference within the circled tornadic region. The RRVDs at different scales are calculated

using (7) and are shown in Figs. 3b–d. The RRVDs at the location of tornado are again larger than 50% and significantly higher than those in other regions at all three scales. The size of the region with large RRVD (>0.5) increases with the scale. In contrast to the idealized vortex case, relatively large values of RRVD also exist away from the tornado due to wind shear and convergence in other parts of the flow but their values are generally significantly below 0.5.

e. Impact of the distance of tornado from radar and tornado size on RRVD

As the distance from the tornado to the radar increases, the azimuthal distance at the tornado location increases so that the tornado becomes more poorly resolved in the radar data. The degree of difficulty in unambiguously detecting a tornado also increases. To test the ability of RRVD in providing distinguishing

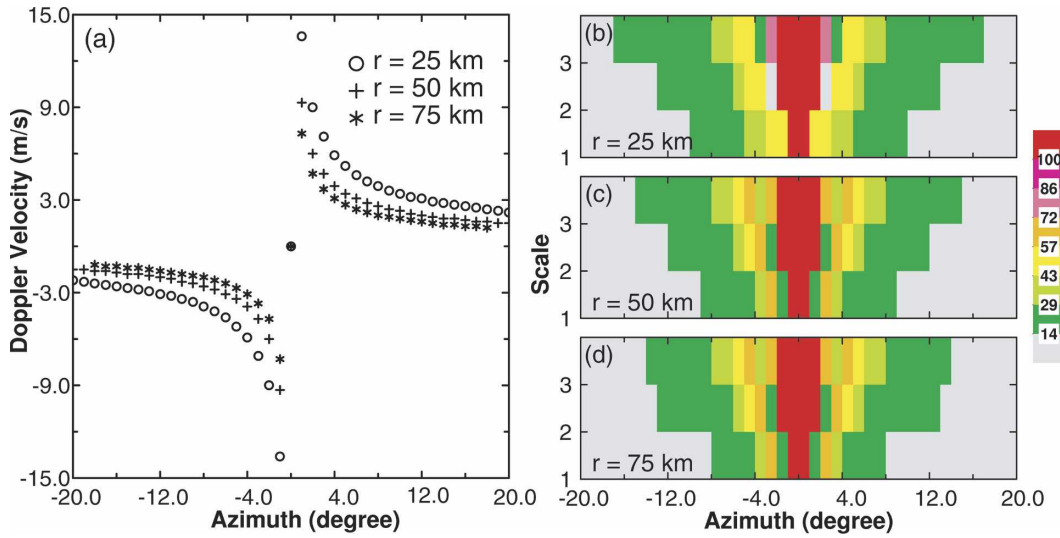


FIG. 4. (a) Sampled radial velocity from modified Rankine combined vortex model and corresponding RRVDs (%) at radar ranges of (b) 25, (c) 50, and (d) 75 km.

information when the tornado is located at larger distances than examined in the previous subsections, we resampled both the idealized and simulated tornadoes, but with the radar located at distances between 20 and 100 km from the tornado, and increased the distance by 5 km from experiment to experiment. In addition, for the case of the idealized tornado, we further decreased the core diameter from the original 400 m to 100 m, to impose more stringent tests on our method. The size of the simulated tornado remained the same.

Figure 4a shows the radial velocities sampled along the constant range circles that pass through the center of the idealized vortex when the radar is located 25, 50, and 75 km away from the tornado. As can be seen, the sampled peak velocities are 13.6, 9.3, and 7.3 m s^{-1} at ranges of 25, 50, and 75 km, respectively, even though the true maximum velocity is 50 m s^{-1} . The RRVDs at the first three scales for the tornado at the three different distances are shown in Figs. 4b, 4c, and 4d. Clearly, the RRVDs near the center of the vortex are larger than 50% for all three scales and all three ranges. It is found that for this idealized tornado, even when the range is 100 km, the RRVDs still show very distinguishable characteristics in the region of the tornado.

The effectiveness of RRVD with the more realistic numerically simulated tornado is further examined for different radar ranges. The radial velocity field sampled by a radar located 60 km west of the tornado and the corresponding RRVDs at the first three scales are shown in Fig. 5. At this range, the sampling volume or pixel appears rectangular, with its azimuthal width being much broader than the range gate length (Fig. 5a), and only a single positive–negative radial velocity cou-

plet shows up near the vortex center. The incoming and outgoing peak velocities near the tornado center are about -6 and 10 m s^{-1} , respectively. The TVS is therefore rather weak. However, the presence of a tornado can still be revealed by RRVDs at all three scales (Figs. 5a–c); the largest RRVDs show up in the tornado region at all three scales. We further found that even when the radar range is larger than 70 km, large RRVDs still show up in the tornado region, but a strong enough TVS cannot be identified from the radial velocity field, making the detection more difficult or less reliable. The 70-km range corresponds to an EBW to core diameter ratio of about 8.5. This suggests that for this realistic simulated tornado, when this ratio is smaller than 8.5, RRVD can be a useful and effective parameter.

In summary, the general formulation of the wavelet analysis is first introduced in this section. The wavelet transform based on a 2D Haar wavelet function is then applied to the radar radial velocity fields associated with two examples of tornado vortices to quantify the relatively region-to-region velocity difference (RRVD) at different scales. For both examples, it is found that 1) in the wavelet domain the tornado vortex is generally associated and collocated with large values of RRVD, 2) the large values of RRVD (>0.5) usually exist at more than one scale, and 3) the size of the region with large RRVD (>0.5) typically increases with the wavelet scale. These characteristics of RRVD are reliable until the ratio of the EBW to the core diameter of the tornado exceeds 8.5 for a tornado with a 55 m s^{-1} peak velocity difference. This ratio is usually larger for tornadoes with a larger peak velocity difference. These

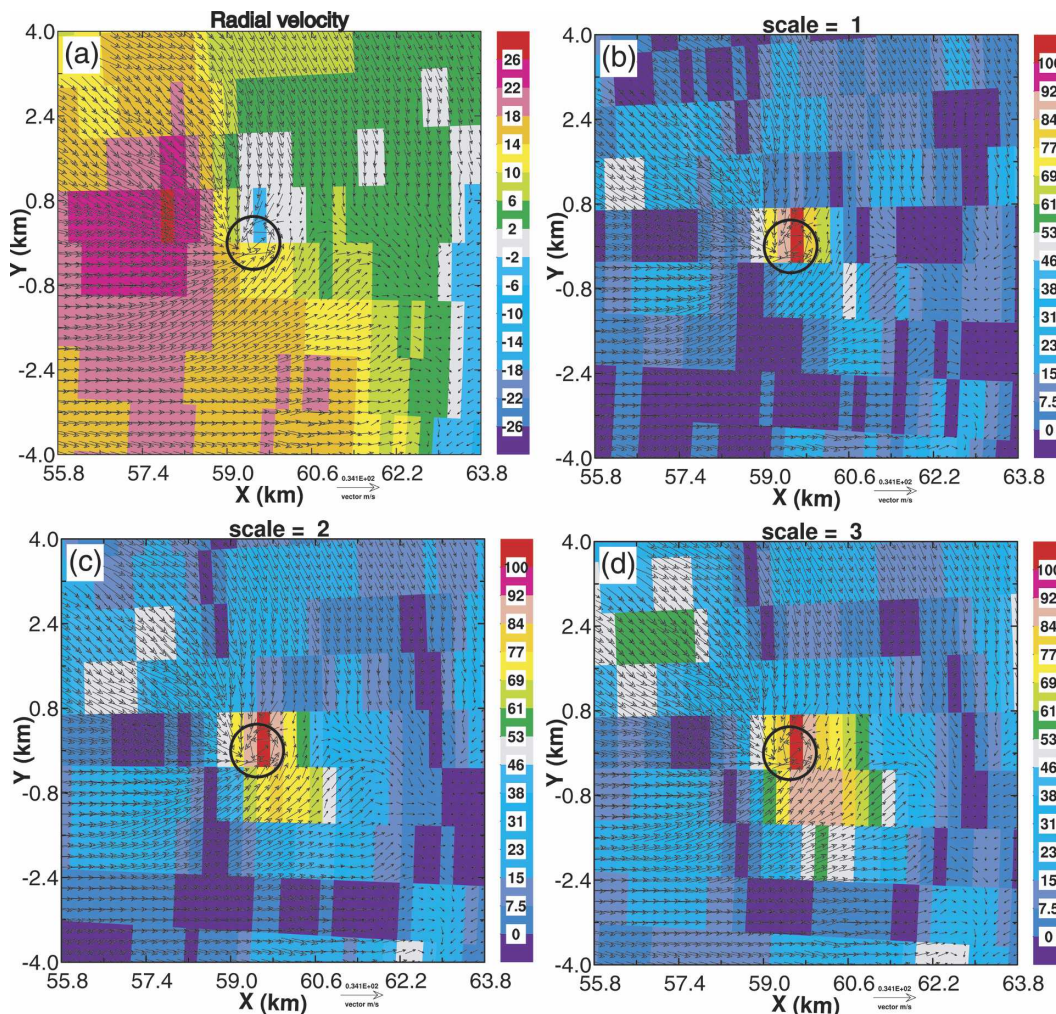


FIG. 5. As in Fig. 3, but for a radar located 60 km west of the tornado.

characteristics will be used to help identify tornadoes in the next section.

3. Tornado detection based on wavelet analysis

We present in this section a wavelet-based tornado detection algorithm, which we call WTDA for short, by using RRVDs calculated for different scales combined with other criteria. If only the RRVD at the smallest scale is used, it becomes similar to algorithms based on the gate-to-gate velocity difference (GVD) or azimuthal shear. As demonstrated in the last section, the RRVD is rather effective in identifying regions of strong shear, and it can do so at different scales. It is therefore chosen as our primary identification parameter (ID). However, the RRVD alone is usually insufficient to uniquely and reliably identify tornado vortices without additional information. Two additional identification parameters are also used in our algorithm. They are, respectively, the mean reflectivity (MRF) and

the region-to-region radial velocity difference (RVD) averaged over the same region as that of RRVD at the corresponding scale. An MRF value larger than 0 dBZ (Mitchell et al. 1998) is required because strong and well-organized tornadoes rarely occur in the case of reflectivity below 0 dBZ and radial velocity measurements are usually not reliable in the absence of reflectivity of sufficient decibel strength. RVD is required to be larger than a threshold value, which is currently set for the smallest scale to be the minimum required shear velocity difference of 11 m s^{-1} as in NTD. Typically, RVD at larger scales tends to be smaller, and its threshold is therefore set to 9 and 8 m s^{-1} at scales 2 and 3, respectively. Additional idealized experiments were performed to determine the proper choice of RVD threshold values. It is found that for an idealized tornado with a maximum rotational velocity of 50 m s^{-1} , even when the core diameter is as small as 100 m and the radar is at the far range of 100 km, the RVDs at the

first three scales are still larger than these thresholds. The function of the RVD parameter is somewhat similar to that of the 2D features used by Mitchell et al. (1998), which were constructed from at least three shear segments. A shear segment is a velocity pair between adjacent beams whose velocity difference exceeds an adaptable but specified threshold. However, the 2D feature does not really examine the wind shear in two dimensions but the shear between adjacent beams, in the azimuthal direction only, while the RVD better represents 2D features by examining the wind shear in square regions of different scales. The MRF and RVD requirements are designed to exclude regions where the RRVDs are large but there is no wind rotation of significant strength.

A flowchart of this algorithm is given in Fig. 6 to show how the WTDA is implemented based on, for example, the WSR-88D level-II data. The first step of the algorithm is the quality control (QC) of raw radar data, which includes unfolding aliased radial velocities, removing clutters, range-fold data, and other quality-related problems (Liu et al. 2003; Zhang et al. 2005; Liu et al. 2005). This step is important in avoiding data quality related false detections (Mitchell et al. 1998). After the QC step, missing values of the radial velocity are filled in with the median of the four adjacent range gates as is done in Smith et al. (2003) if the number of continuously missing measurements along a beam is less than 3.

The second step is to calculate the three ID parameters for each of the three smallest scales. Based on our earlier examinations of idealized and simulated tornadoes, large values of RRVD exist at two or more scales in the presence of a tornado, and therefore a scale continuity check is applied in the third step. For a given location, if the RRVD exceeds a specified threshold, for example, 0.5, in any two adjacent scales, the location of the corresponding pixel or sampling volume is saved. Note that the threshold of RRVD is an adjustable parameter. In this paper, the threshold is specified to be 0.5 based on the cases of idealized and simulated tornadoes examined in the previous section. An RRVD value larger than 0.5 implies that the radial wind shear in the region is relatively large at the corresponding scale. Thus, such regions deserve special attention.

The pixels or sampling volumes saved in step 3 are further checked for their values of MRF and RVD. If MRF is smaller than 0 dBZ or any of the RVDs at the first three scales are smaller than their thresholds, the pixel is discarded. The fifth step builds 2D groups from the remaining qualifying pixels. Each pixel is first considered as an individual group. If the distance between

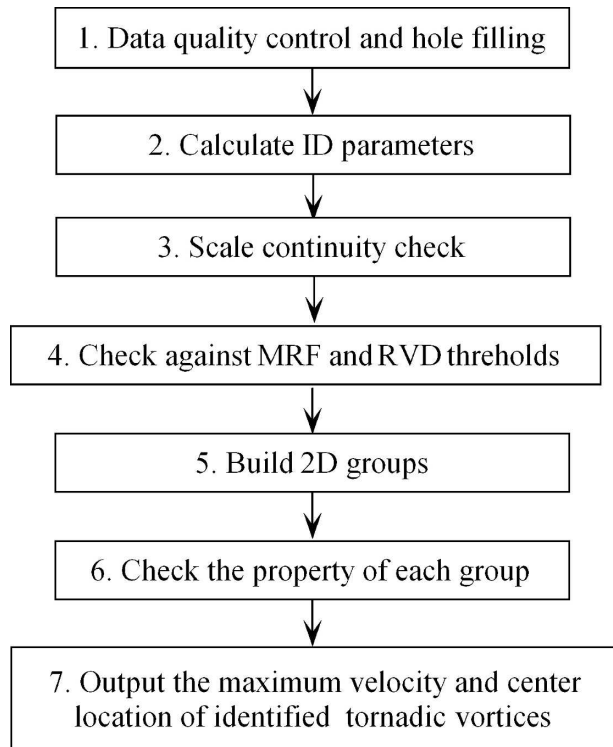


FIG. 6. Flowchart of the wavelet-based tornado detection algorithm.

two groups is smaller than two range-gate or azimuthal intervals, they are combined into the same group. This process is repeated until the distance between any two groups is larger than two gate intervals. The sixth step checks the properties of each group. We require that the mean reflectivity, which is averaged over all valid observations in each group, is larger than 0 dBZ, and further the peak incoming and outgoing velocities are larger than 6 m s^{-1} and that there exists a sign change in the radial velocity in the azimuth direction to ensure that the vortex is produced by incoming and outgoing radial velocities. The groups that pass all the above checks will be considered tornadic. The location of the group center is defined as the center of the tornado. The maximum radial velocity and the center location for each of the tornadic vortices are then recorded.

As mentioned earlier, in our algorithm, the RRVD at the smallest scale is similar to the velocity difference between adjacent velocity gate pairs, the key identifier in the NTDA. However, as discussed in the introduction, calculating shear from two data points can be unreliable due to radar data noise arising from data quality problems related to, for example, receiver saturation and moving clutter targets (Zittel et al. 2001). Such radar data quality problems are difficult to eliminate in level II data. Natural small-scale variations in the flow

fields can also create representativeness problems with the GVD calculations (Desrochers and Yee 1999), thereby causing false alarms. On the other hand, large GVDs due to data noise tend to be random and localized and their spatial scales are small. Such localized problems tend to be filtered out effectively in the wavelet components of larger scales. As was shown in section 3, the information about the tornado usually exists at more than one wavelet analysis scale in the radial velocity data, and when a tornado is present, it is often identifiable at all three of the smallest scales in the normalized wavelet amplitudes, or RRVD in our case. When the scale continuity check is applied, features due to small-scale data noise can be filtered out effectively, thereby reducing the false alarm rate. As discussed in the introduction, the use of multiple data points in the local, linear least square estimation of the velocity derivative in the work of Smith et al. (2003) and Smith and Elmore (2004) serves a somewhat similar purpose, although the actual approach is different.

It should be pointed out here that Desrochers and Yee (1999) also applied wavelet analysis to vortex detection and, in their case, to the detection of mesocyclones. In their method, the wavelet analysis is used to remove small-scale variations and fill data gaps so that the mesocyclone-related signals can be retained at the scales of interest. Therefore, the purpose of their application is very different from ours.

In addition, as pointed out by Desrochers and Yee (1999), traditional tornado detection algorithms do not identify the 2D features of the velocity couplet directly but derive them through 1D azimuthal shear segments. This is a factor that potentially increases the false alarm rate (Lee and White 1998). In this paper, the velocity couplet is described in terms of the region-to-region velocity difference and RRVD directly measures the 2D radial wind shear at each point and detects the velocity couplet instead of 1D shear segments. Also, because the size of tornado vortices varies from tens of meters to 1–2 km, the traditional detection algorithms often have difficulties in defining suitable criteria for constructing 2D features from 1D azimuthal shear segments. The mesocyclone detection algorithms (MDAs) often misidentify a tornado vortex as a mesocyclone when the tornado is close to a radar and misidentify a mesocyclone as a tornado when the mesocyclone is far away. On the other hand, traditional tornado detection algorithms do not attempt to identify mesocyclones. Because our WTDA identifies 2D features in terms of the wavelet functions representing different scales, it may provide a natural way for combining MDA and TDA. This can be an area of future research.

4. Testing of WTDA with the 8 May 2004 central Oklahoma tornado case

a. Statistical characteristics of RRVD

The real test of any detection algorithm should be against real tornado cases. Radar data collected by the Oklahoma City, Oklahoma, WSR-88D (KTLX) on 8 May 2003 are used to examine the performance of our detection algorithm. On that day, a weak supercell tornado (F0) formed at 2206 UTC about 20 km south of the KTLX radar. It reached an intensity of F4 by 2220 UTC but dissipated by 2236 UTC after moving to about 15 km northeast of the KTLX radar. The tornado traveled for about 27 km on the ground (NCDC 2003). This tornado was observed by the radar in a series of seven volume scans. A good description of the case can be found in Burgess (2004). In each volume scan, the tornado core region in the lowest elevation of KTLX data is subjectively identified for verification purposes.

To examine the statistical characteristics of radial velocity data within the tornadic and nontornadic regions, we separate the radar observations in the lowest elevation into two groups. The observations within the tornado region are classified into group I, which contains 147 observations from the seven lowest elevations. The gate-to-gate check of the NTDA is applied to the nontornadic regions. If the velocity difference is larger than 11 m s^{-1} , the corresponding radar observations are classified into group II so that they will be examined by the detection algorithm (those with smaller velocity differences are ignored). Here, the 11 m s^{-1} threshold is that used in NTDA (Mitchell et al. 1998). Group II contains 9352 observations. As can be seen, the number of observations in group II is far larger than that in group I. All data points in group II should eventually be discarded by the tornado detection algorithm as we know they are not tornadic. It will be shown that the WTDA is more effective in eliminating data points in group II based on the statistical features of the two groups of data.

When the wavelet transform is applied to each sweep of radar observations, RRVD can be calculated according to Eq. (7). The frequency histograms of RRVD are plotted for the first three scales in Fig. 7 for group I data and in Fig. 8 for group II data. According to Figs. 7a and 8a, the RRVD values for the smallest scale ($m = 1$) at most of the observation points are smaller than 0.5 in both groups. This indicates that it is difficult to distinguish real tornadic from nontornadic wind shear when using the smallest scale alone. However, as scale index m increases, the difference in the histograms between the two groups becomes larger. In group II, most of the

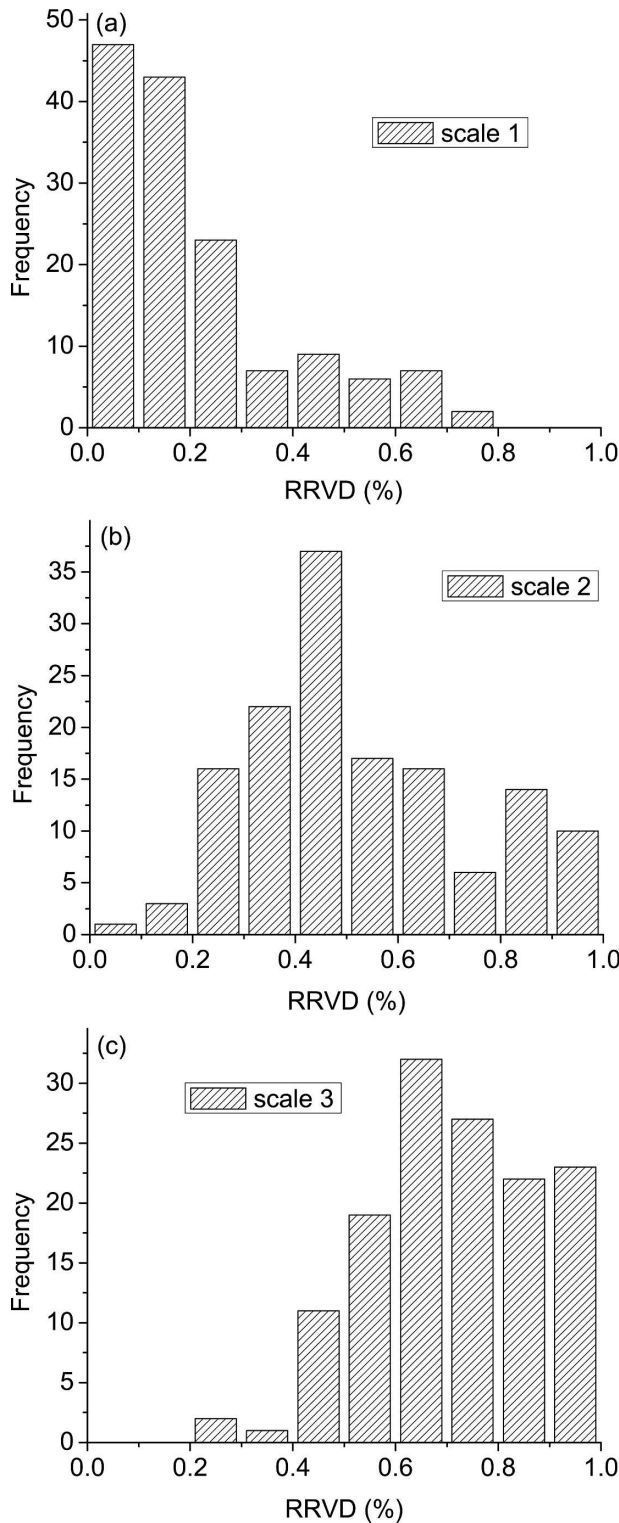


FIG. 7. Frequency histograms of RRVDs for data points in group I (tornadoic shears) at scales $m =$ (a) 1, (b) 2, and (c) 3.

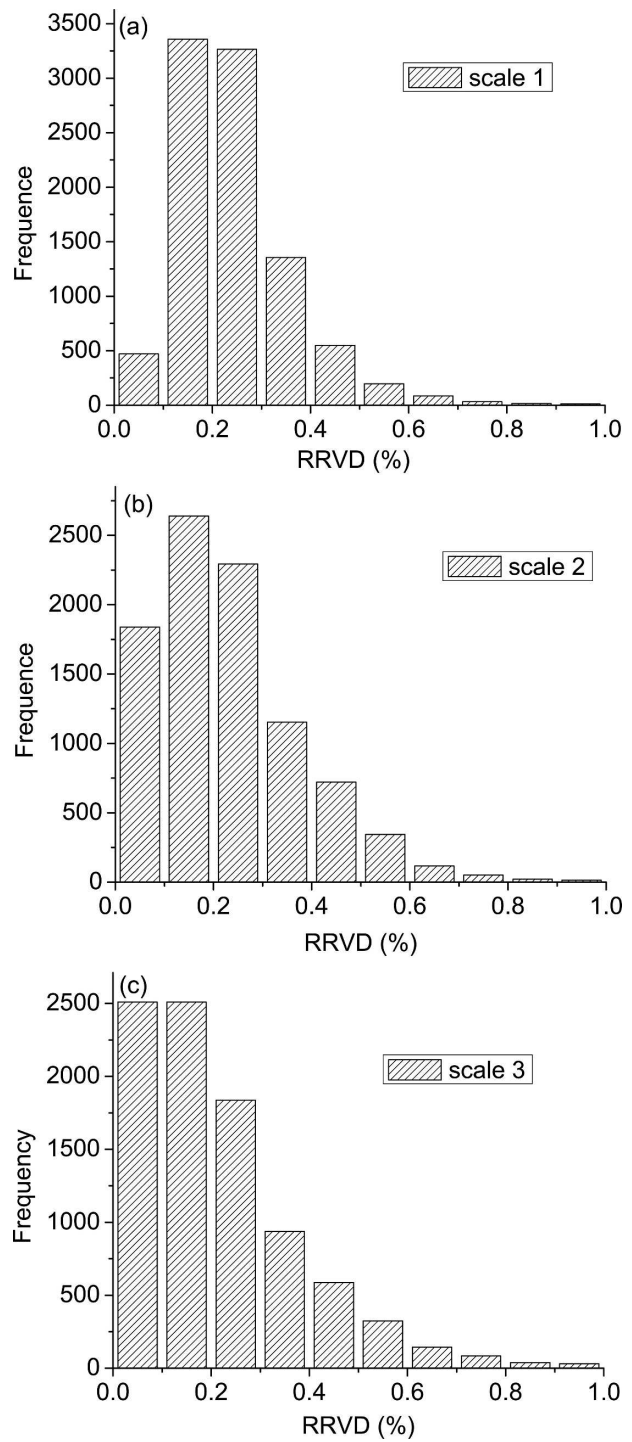


FIG. 8. As in Fig. 7, but for RRVDs for data points in group II (nontornadoic shears).

RRVD values remain in the range of 0–0.5 for scale indices 2 and 3 while a very small percentage (<5%) of values exceed 0.5 for all scales, indicating that at least 95% of nontornadoic shears can be eliminated when a

TABLE 1. The number of remaining 2D features (groups) after an NTDA azimuthal gate-to-gate check, after the WTDA scale continuity check, and finally after all steps in WTDA.

Time UTC	2206	2211	2215	2220	2225	2230	2235
2D features after NTDA check	32	31	41	46	31	46	35
2D groups after scale continuity check	4	8	3	2	6	8	7
2D groups after all WTDA steps	1	3	1	1	1	1	1

RRVD threshold of 0.5 is used. For group I, however, the distribution is increasingly biased toward large values of RRDV as the scale index increases; in fact, for scale index 3, 90% of RRVD values exceed 0.5. These distinctive characteristics exhibited at the different scales between the tornadic (group I) and nontornadic (group II) regions agree with the findings obtained from the earlier idealized and simulated tornado vortex experiments; that is, RRDVs at multiple scales can be very helpful for separating tornadoes from nontornadic shears.

b. Results of the WTDA

The WTDA algorithm is applied to the seven volume scans of data from the KTLX radar that were collected on 8 May 2003 to test the effectiveness of the algorithm. To examine the effectiveness of the scale continuity check in rejecting nontornadic shears as compared to the 2D feature construction and elimination procedure in the NTDA, the number of 2D features initially identified by the NTDA procedure and that of 2D groups identified after our scale-continuity check are calculated.

A 2D feature is composed of at least three shear segments. Constructing 2D features is a way of eliminating nontornadic shear features by checking the 2D spatial continuity performed in NTDA. The numbers of constructed 2D features in all seven scans examined are listed in the first row of Table 1. In NTDA, the number of constructed 2D features in each lowest scan is no less than 30. This implies that the tornado-like 2D features have to be eliminated by other steps, such as the 3D feature construction step performed in NTDA, which uses data from more elevations. This step tends to be sensitive to the number of elevations available, which mostly depends on the distance of the tornado from the radar. In addition, we found that the 2D feature check used in NTDA actually missed the true tornadic feature at 2235 UTC among a total of 35 two-dimensional features it identified.

A scale continuity check is one of the ways of eliminating nontornadic shear in WTDA. We show here that most of the nontornadic shears can be eliminated by our scale continuity check using the lowest-elevation

scan only. The number of 2D groups remaining after the scale continuity check is counted and listed in the second row of Table 1. After the check, the remaining number of 2D groups in all scans is no more than eight and all true tornadic features are found to remain. The scale continuity check is therefore very effective in eliminating nontornadic features while keeping the tornadic ones.

We note here that NTDA does include additional steps, including the construction of 3D features using more elevations, which will also eliminate some of the 2D features listed in the first row of Table 1. This step can also be applied in our algorithm, although we hope that 3D feature checking can be more effectively achieved by performing in the future 3D wavelet analysis.

Most of the remaining nontornadic 2D groups can be further eliminated by the ensuing steps in our algorithm; this is illustrated below for one scan time. The numbers of remaining 2D groups after passing through all steps in WTDA are listed in the third row of Table 1 for different times. All true tornadic shears in the scans during this test period except that at 2211 UTC are identified uniquely by WTDA, while the two nontornadic shears remaining at 2211 UTC after all check steps of WTDA are caused by ground clutter.

An example of applying our WTDA algorithm to the data from the KTLX radar is shown in Fig. 9. Figure 9a shows the observed radial velocity field roughly between the 10- and 20-km-range circles at 2220 UTC 8 May 2003. Nine 2D features in total are identified by NTDA in the plotted region in Fig. 9a and they are marked by small labeled circles. Among these, only the circle labeled 1 is the location of a true tornado, while the other features are caused by, for example, data noise and data quality problems.

The corresponding fields of the RRVD at the first three scales are plotted in Figs. 9b–d. As shown in Fig. 9b, RRVD is larger than 0.5 at circles 1, 6, 7, and 8 but small at other circles. This means that the other five nontornadic 2D features have been effectively eliminated even when using RRDVs for the smallest scale only. Note that at scale 1, both the maximum value of RRDVs and the area coverage of the values exceeding

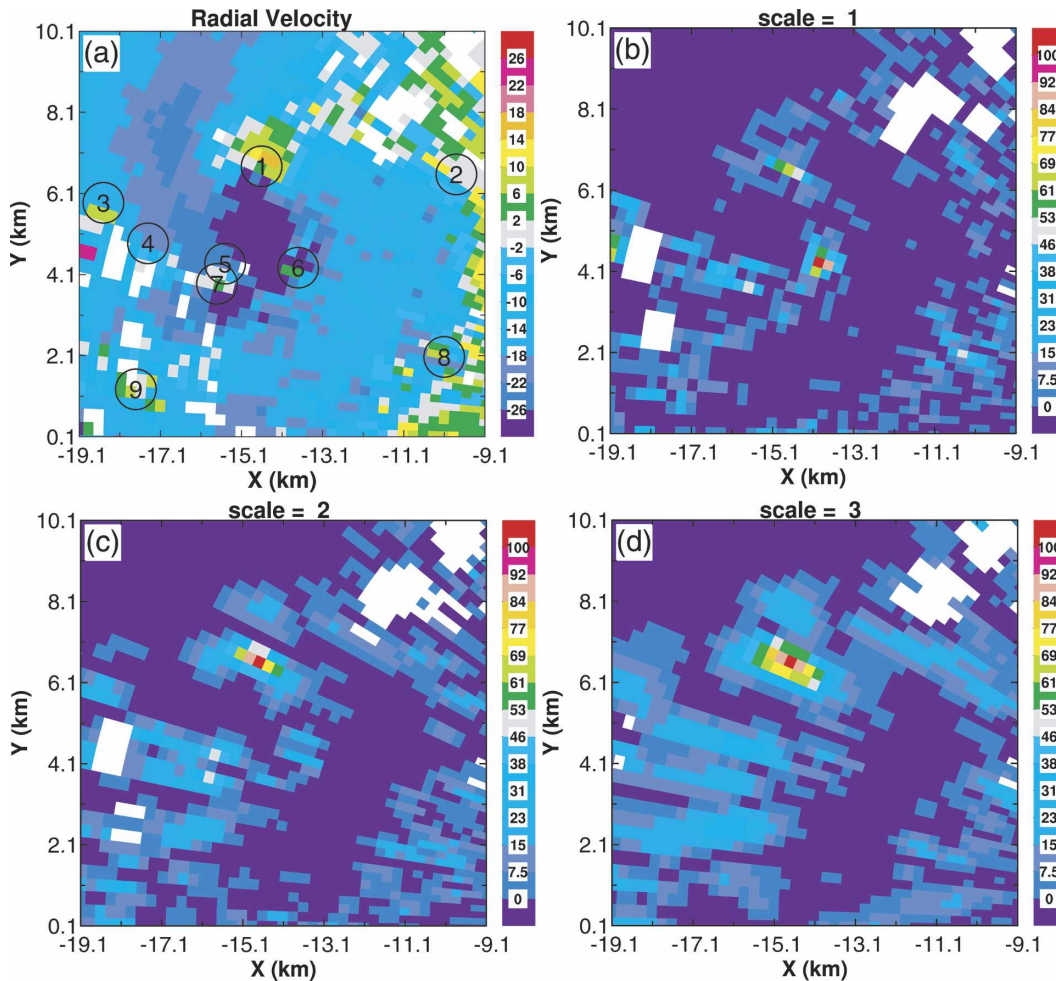


FIG. 9. (a) Radar radial velocity field observed by the KTLX radar at 2220 UTC 8 May 2003, and the corresponding RRVD (%) at scales $m =$ (b) 1, (c) 2, and (d) 3.

0.5 are larger for circle 2 than for circle 1, where the true tornado is located. This hints at the unreliability of RRVD at the smallest scale, which is closest to the gate-to-gate shear. Starting from scale 2, the feature associated with the true tornado becomes clearly dominant in term of the RRVD value. At scale 2, the feature associated with circle 7 is still identifiable (Fig. 9c) but all other features (circles 6 and 8) become very weak relative to the background values. In particular, all values of RRVD in circle 6 becomes smaller than 0.5, and thus this nontornadic feature arising from data noise is eliminated. At scale 3, only the tornadic feature is clearly identifiable. Thus, there are two features (circles 1 and 7) that pass the scale continuity check. When we further examine the group property of the remaining features in step 6, there is no sign change for the radial velocity in the group that is indicated by circle 7. Thus, the nontornadic feature 7 can be discarded by the ensuing steps in the WTDA. The above

example demonstrates that the scale continuity check is able to successfully eliminate most of the nontornadic features identified by simple gate-to-gate shear checking.

5. Summary and conclusions

In this paper, wavelet analysis is applied to the detection of tornadoes from Doppler radial velocity observations. A tornado detection algorithm is developed based on the wavelet analysis (called WTDA) as a proof of concept. The scale- and location-dependent wavelet coefficients derived from the radial velocity field are used to define a relative region-to-region velocity difference (RRVD). The RRVD is shown to effectively describe the 2D region-to-region wind shear at different spatial scales and is therefore used in WTDA as a key discriminating parameter. This is in contrast to the gate-to-gate shears corresponding to the (radar)

grid scale used in typical tornado detection algorithms. Multiscale RRVDs make it more flexible to identify tornadic vortices with less sensitivity to the intensity or size of the tornado and are more effective in eliminating nontornadic shears caused by data noise and/or quality problems.

The wavelet analysis is first applied to radial velocity data sampled from idealized as well as numerically simulated tornadoes, for the purpose of understanding the characteristics of RRVD associated with tornado vortices. It is found that the tornado vortices are collocated with areas where the RRVDs are large and their values usually exceed 0.5 at more than one scale. Based on these characteristics, the WTDA is developed using RRVD as the primary identification parameter. The WTDA is further tested with WSR-88D data from an 8 May 2003 central Oklahoma tornado case. The scale continuity check in the WTDA, in terms of the RRVDs, is found to be effective in eliminating nontornadic shears.

The effectiveness of RRVD is also examined by looking at a smaller idealized tornado, and sampling the tornadoes from longer ranges. It is found that when the ratio of the azimuthal distance between two adjacent constant-range gates to the tornado core diameter is smaller than 8.5 for a relatively weaker tornado, RRVD can provide very useful information for tornado detection. The WTDA was further applied to the 10 May 2003 Oklahoma tornado case (results not presented in this paper) to examine the capability of WTDA for a tornado at a larger distance. In this case, an F1 tornado started at 0525 UTC and ended at 0533 UTC and traveled for about 2 mi on the ground. The core diameter of the tornado was about 280 m (NCDC 2003) and the tornado was observed by the KTLX radar at a range of about 90 km at 0528 UTC. The WTDA was applied to the lowest-elevation scans around this time and the results show that after a scale continuity check, only four 2D features remained and the tornado was also correctly identified after ensuing steps in the WTDA algorithms.

The thresholds used for the other identification parameters in WTDA are specified based mostly on previous papers (e.g., Mitchell et al. 1998) and the experience of the authors. These thresholds worked the best for the cases examined in this paper as well as for the tornado case of 3 May 1999 near Oklahoma City (results not shown in this paper). Optimal values for a wide variety of cases would require testing against a large radar dataset and tornado database. This is planned for the future but we believe the examples shown in this paper serve the proof-of-concept purpose that demonstrates the efficacy of the wavelet analysis.

In addition, the current WTDA algorithm does not include a continuity checking across the elevations and it is believed that the vertical check, when implemented in the future, can further improve the reliability of the algorithm. We may also seek to implement wavelet analysis in the vertical direction and apply the concept used in the elevation plane to three dimensions. At the same time, the fact that our multiscale wavelet-based algorithm does a reasonably good job without multielevation data represents an important advantage, especially for radars not operating in conventional sit-and-spin modes. The latter include mobile radars that often focus on the low levels, and the dynamically adaptive radars of the Engineering Research Center for Collaborative Adaptive Sensing of the Atmosphere (CASA). The rapid detection of tornadoes and other low-level hazardous weather and the use of the detection information to adaptively steer the scanning of its network of radars are important goals of CASA (see, e.g., Xue et al. 2006).

Since no direction comparisons have been performed against a large enough tornado database, we do not claim the superiority of our WTDA over any of the existing, established tornado detection algorithms. The need for tuning and refinement of our algorithms is expected when we test the algorithm against a large enough dataset. Eventually, we want to implement our algorithm within the NSSL Warning Decision Support System-Integrated Information (WDSS-II) system and perform side-by-side comparisons with the NSSL TDA to further evaluate the performances of WTDA. In addition, the scale-dependent parameter RRVD developed in this paper can also be used as a parameter in probabilistic tornado detection algorithms, in a manner similar to that done in Lakshmanan et al. (2005).

Acknowledgments. This work was primarily supported by NSF Grant EEC-0313747 of the Engineering Research Center Program to CASA. S. Liu and M. Xue were also supported by an FAA grant via DOC-NOAA NA17RJ1227 and M. Xue further by NSF Grants ATM0129892, ATM-0331594, and ATM-0331756. Q. Xu acknowledges the support provided by FAA Contract IA# DTFA03-01-X-9007, as well as ONR Grants N000140310822 and N000140410312. Jerry Brotzge is thanked for proofreading and commenting on the original manuscript.

REFERENCES

- Brown, R. A., 1998: Nomogram for aiding the interpretation of tornadic vortex signatures measured by Doppler radar. *Wea. Forecasting*, **13**, 505–512.
- , L. R. Lemon, and D. W. Burgess, 1978: Tornado detection by pulsed Doppler radar. *Mon. Wea. Rev.*, **106**, 29–38.

- , V. T. Wood, and D. Sirmans, 2002: Improved tornado detection using simulated and actual WSR-88D data with enhanced resolution. *J. Atmos. Oceanic Technol.*, **19**, 1759–1771.
- Browning, K. A., 1965: The evolution of tornadic storms. *J. Atmos. Sci.*, **22**, 664–668.
- Burgess, D. W., 2004: High resolution analyses of the 8 May 2003 Oklahoma City storm. Part 1: Storm structure and evolution from radar data. Preprints, *22d Conf. on Severe Local Storms*, Hyannis, MA, Amer. Meteor. Soc., CD-ROM, 12.4.
- , L. R. Lemon, and R. A. Brown, 1975: Tornado characteristics revealed by Doppler radar. *Geophys. Res. Lett.*, **2**, 183–184.
- Crum, T. D., and R. L. Alberty, 1993: The WSR-88D and the WSR-88D Operational Support Facility. *Bull. Amer. Meteor. Soc.*, **74**, 1669–1687.
- Daubechies, I., 1992: *Ten Lectures on Wavelets*. CBMS-NSF Regional Conference Series in Applied Mathematics, Vol. 61, SIAM, 357 pp.
- Desrochers, P. R., and R. J. Donaldson Jr., 1992: Automatic tornado prediction with an improved mesocyclone-detection algorithm. *Wea. Forecasting*, **7**, 373–388.
- , and S. Y. K. Yee, 1999: Wavelet applications for mesocyclone identification in Doppler radar observations. *J. Appl. Meteor.*, **38**, 965–980.
- Forbes, G. S., 1981: On the reliability of hook echoes as tornado indicators. *Mon. Wea. Rev.*, **109**, 1457–1466.
- Fujita, T., 1958: Mesoanalysis of the Illinois tornadoes of 9 April 1953. *J. Meteor.*, **15**, 288–296.
- Lakshmanan, V., I. Adrianto, T. Smith, and G. Stumpf, 2005: A spatiotemporal approach to tornado prediction. *Int. Joint Conf. on Neural Networks*, Vol. 3, Montreal, QC, Canada, IEEE, 1642–1647.
- Lee, R. R., and A. White, 1998: Improvement of the WSR-88D mesocyclone algorithm. *Wea. Forecasting*, **13**, 341–351.
- Liu, S., P. Zhang, L. Wang, J. Gong, and Q. Xu, 2003: Problems and solutions in real-time Doppler wind retrievals. Preprints, *31th Conf. on Radar Meteorology*, Seattle, WA, Amer. Meteor. Soc., 308–309.
- , Q. Xu, and P. Zhang, 2005: Identifying Doppler velocity contamination caused by migrating birds. Part II: Bayes identification and probability tests. *J. Atmos. Oceanic Technol.*, **22**, 1114–1121.
- Mitchell, E. D., S. V. Vasiloff, G. J. Stumpf, A. Witt, M. D. Eilts, J. T. Johnson, and K. W. Thomas, 1998: The National Severe Storms Laboratory Tornado Detection Algorithm. *Wea. Forecasting*, **13**, 352–360.
- NCDC, cited 2003: Storm event. [Available online at <http://www4.ncdc.noaa.gov/cgi-win/wwwcgi.dll?wwEvent~Storms>.]
- Smith, T. M., and K. L. Elmore, 2004: The use of radial velocity derivatives to diagnose rotation and divergence. Preprints, *11th Conf. on Aviation, Range, and Aerospace*, Amer. Meteor. Soc., Hyannis, MA, CD-ROM, P5.6.
- , —, G. J. Stumpf, and V. Lakshmanan, 2003: Detection of rotation and boundaries using two-dimensional, local, linear least squares estimates of velocity derivative. Preprints, *31st Conf. on Radar Meteorology*, Seattle, WA, Amer. Meteor. Soc., 310–314.
- Vasiloff, V. S., 2001: Improving tornado warnings with the Federal Aviation Administration's Terminal Doppler Weather Radar. *Bull. Amer. Meteor. Soc.*, **82**, 861–874.
- Wieler, J. G., 1986: Real-time automated detection of mesocyclones and tornadic vortex signatures. *J. Atmos. Oceanic Technol.*, **3**, 98–113.
- Wood, V. T., and R. A. Brown, 1997: Effects of radar sampling on single-Doppler velocity signatures of mesocyclones and tornadoes. *Wea. Forecasting*, **12**, 928–938.
- Xue, M., K. K. Droegemeier, and V. Wong, 2000: The Advanced Regional Prediction System (ARPS)—A multiscale nonhydrostatic atmospheric simulation and prediction tool. Part I: Model dynamics and verification. *Meteor. Atmos. Phys.*, **75**, 161–193.
- , and Coauthors, 2001: The Advanced Regional Prediction System (ARPS)—A multiscale nonhydrostatic atmospheric simulation and prediction tool. Part II: Model physics and applications. *Meteor. Atmos. Phys.*, **76**, 143–165.
- , M. Tong, and K. K. Droegemeier, 2006: An OSSE framework based on the ensemble square-root Kalman filter for evaluating impact of data from radar networks on thunderstorm analysis and forecast. *J. Atmos. Oceanic Technol.*, **23**, 46–66.
- Zhang, P., S. Liu, and Q. Xu, 2005: Identifying Doppler velocity contamination caused by migrating birds. Part I: Feature extraction and quantification. *J. Atmos. Oceanic Technol.*, **22**, 1105–1113.
- Zittel, W. D., R. R. Lee, E. D. Mitchell, and D. Sirmans, 2001: Environmental and signal processing conditions that negatively impact the performance of the WSR-88D tornado detection algorithm. Preprints, *30th Conf. on Radar Meteorology*, Munich, Germany, Amer. Meteor. Soc., 310–314.